Electronic Structures of Mono-Oxidized Copper and Nickel Phosphasalen Complexes

Irene Mustieles marín, Thibault Cheisson, Rohit Singh-Chauhan, Christian Herrero, Marie Cordier, Carine Clavaguera, Grégory Nocton, Audrey Auffrant

Electronic Structures of Mono-Oxidized Copper and Nickel Phosphasalen Complexes

Irene Mustieles Marín,[a] Thibault Cheisson,[a] Rohit Singh Chauhan,[a] Christian Herrero,[c] Marie Cordier,[a] Carine Clavaguéra,[a,b]* Grégory Nocton,[a]* and Audrey Auffrant [a]*

Abstract: Non-innocent ligands render the determination of the electronic structure in metal complexes difficult. A combination of experimental techniques and quantum chemistry are required to correctly elucidate it. This paper deals with the one-electron oxidation of copper(II) and nickel(II) complexes featuring phosphasalen ligand (Psalen), which differs from their salen analogues by the presence of iminophosphorane groups (P=N) instead of imines. Various experimental techniques (X-ray diffraction, cyclic voltammetry, NMR, EPR, and UV-vis spectroscopies, and magnetic measurements) as well as quantum chemistry calculations were used to define the electronic structure of the oxidized complexes. This can be deeply modified by a small change in the ligand structure, *i.e.* the replacement of a *tert*-butyl group by a methoxy on the phenoxide ring. The different techniques have allowed quantifying the amount of spin density located on the metal center and on the Psalen ligands. All complexes were found to possess a multi-configurational ground state, in which the ratio of the +II *vs*. +III oxidation state of the metal center, and therefore the phenolate *vs*. phenoxyl radical ligand character, varies upon the substituents. The *tert*-butyl group favors a strong localization on the metal center whereas with the methoxy group the metallic configurations decrease and the ligand configurations increase. The importance of the geometrical considerations compared with the electronic substituent effect is highlighted by the differences observed between the solid-state (EPR, magnetic measurements) and solution characterizations (EPR and NMR data).

Introduction

Transition metal complexes bearing so-called non-innocent ligands[1] have recently become an area of intensive research.[2] In these systems, a redox event can take place either on the ligand and/or the metal, which drastically complicates the assignment of the oxidation state of the metal. Di-imine, phenolamine, catechol or phenol based ligand systems[3] are examples of such non-innocent ligands. Thus, Chirik and Wieghardt elegantly demonstrated how bis-iminopyridines can act as electron reservoirs “conferring nobility to base metals”,[4] opening the way to new reactivity and catalytic reactions.[2a, 5] Bio-inorganic systems, such as the cytochrome P450 or the galactose oxidase enzyme, often possess redox-active ligands. As an example, galactose oxidase, which catalyzes the aerobic oxidation of primary alcohols in aldehydes, was shown to incorporate a copper(II) center and a tyrosine radical in its active site. In 1998, one-electron oxidized copper(II) salen complexes characterized as phenoxyl radical complexes were proved to behave as functional biomimetic models of the galactose oxidase.[6]

Complexes containing salen ligands have attracted the interest of numerous research groups because of the many different possible variations of the ligand backbone and its electronic structure, which combines donating oxygen atoms and withdrawing imine moieties.[3a, 7] Therefore, this family of ligands allows many different redox situations. Additionally, intramolecular electron transfers are also possible and have contributed to the popularity of this ligand family. Because of the relative energy of the low-lying imine empty π orbitals, a reductive metal center will be stabilized, but if the reduction potential is too low, an electron transfer occurs followed by typical radical coupling.[8] On the other hand, oxidative metal centers will readily allow the formation of an electronic structure in which a delocalized electronic hole is created on the ligand.[3a,9] This latter consideration is relevant for the galactose oxidase electronic structure[10] and was largely studied.[11]

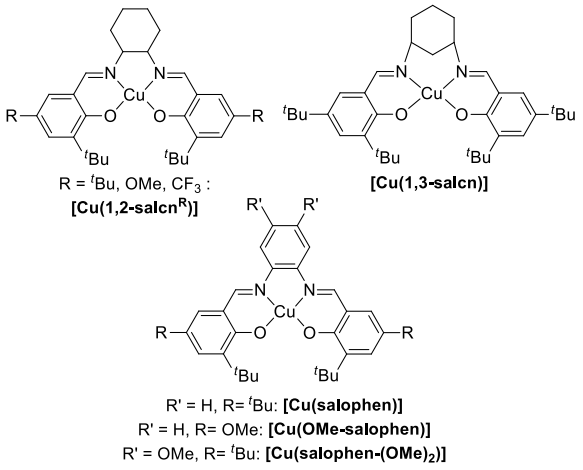

Figure 1. Structures of some salen and salophen copper complexes.

[a] I. Mustieles Marín, Dr. T. Cheisson, Dr. R. Singh-Chauhan, M. Cordier, Dr. C. Clavaguéra, Dr. G. Nocton, Dr. A. Auffrant
LCM
CNRS-Ecole polytechnique, Université Paris-Saclay,
F-91128 Palaiseau Cedex
E-mail: greg.nocton@polytechnique.edu,
audrey.auffrant@polytechnique.edu

[b] Dr. C. Clavaguéra
Laboratoire de Chimie Physique
CNRS - Université Paris-Sud, Université Paris-Saclay,
15 avenue Jean Perrin, 91405 Orsay, France
E-mail: carine.clavaguera@u-psud.fr

[c] Dr. C. Herrero
Institut de Chimie Moléculaire et des Matériaux d’Orsay
UMR 8182 CNRS - Univ. Paris-Sud, Univ. Paris Saclay,
91405 Orsay Cedex, France.
Supporting information for this article is given via a link at the end of the document.

Examples of copper and nickel complexes bearing various salen ligands have been reported over the last decade, each one exhibiting a different electronic structure (Figure 1). For **[Cu(1,2-salcn^{tBu})]**, a Cu^{III} complex was characterized in the solid-state whereas a reversible spin-equilibrium between a ligand radical species and a high valent complex was suggested in solution.[12] In **[Cu(1,2-salcn^{OMe})]** (Figure 1), the introduction of a better donor, led to a partially localized copper(II) radical salen complex after oxidation.[13] Whereas with an electron-withdrawing CF_3 group, a Cu^{III} center was evidenced below 233 K.[14] Subtle modifications such as the use of **1,3-salcn** chelate in place of **1,2-salcn** (Figure 1) altered the electronic structure of the mono-oxidized derivative, which was described as a ligand radical complex both in solution and in the solid-state. The incorporation of an aromatic ring within the ligand backbone allowed upon oxidation the formation of an *o*-diiminobenzene radical in the case of **[Cu(salophen-(OMe)$_2$)]** whereas for **[Cu(salophen)]** and **[Cu(OMe-salophen)]** the phenoxyl radical was favored.[15]

The fast development of these so-called redox non-innocent ligands[2a, 16] shed light on many studies aiming at better understanding the reasons leading to unusual electronics, and very recent reports feed the debate on high valent late transition metals.[17] In particular, considerable efforts in the synthesis and characterization of high valent copper(III) and nickel(III/IV) complexes have been made in recent years. Thus, the groups of Sanford, Mirica and Fout, among others, have reported examples of formally Ni^{IV} complexes,[18] Ni^{III} complexes have found applications in synthetic transformations,[19] while Cu^{III} complexes have very often been proposed as key intermediates.[20] They also have been isolated by different groups[21] and their oxidation state assessed by various spectroscopies.[22] Since the seminal works by Solomon, Cu K-edge X-ray adsorption spectroscopy has often been viewed as the gold standard for the determination of physical oxidation states.[21b] However, recent results from Tomson, Warren, Wieghardt and Lancaster have tempered some of these interpretations.[17a, 23]

The difficulty in determining the oxidation state in transition metal complexes arises from covalency, *i.e.* the orbital overlap,[24] which allows the description of a bonding orbital delocalized over two fragments. The valence of the metal center is given by the formal electron count in this delocalized orbital.[25] If the orbital overlap decreases but the two ionic fragments remain close in energy, the bonding electrons may be spatially located in several different orbitals, allowing the description of several different configurations, in which the oxidation state of the metal center varies.[12, 26] Playing with the relative energy of the two different fragments tends to localize the valence electrons in either one of the configurations: the preponderant configuration[1] is metal-based or ligand-based.[17a] It is also conceivable that different configurations with an identical spin state may all contribute to the electronic ground state of the molecule, allowing a multi-configurational state. Such a situation is particularly well addressed in several lanthanide coordination complexes,[27] which cannot develop orbital overlap with their ligand to a great extent because of the nature of the 4f valence orbitals, then allowing multi-configurational ground states. The relative energy of the different fragments modifies the ratio of the different configurations in the ground state.[28] In transition metals, this questioning has recently been discussed for NO complexes,[29] and for copper-O_2 complexes.[30] Indeed, the possible orbital overlap that allows small mixing of the metal and ligand orbitals does not help in the accurate description of the spectroscopic oxidation state. Therefore, only a careful examination of the electronic structure allows the better description of the spectroscopic oxidation state in metal complexes with so-called redox non-innocent ligands.[31a, b]

Given our interest in electron-rich iminophosphorane (P=N) based ligands as alternatives to imine ones,[32] we began to study the phosphorous analogues of salen, that we termed phosphasalen (or Psalen).[33] In a previous study, we investigated the electronic structure of **[Ni(Psalen^{tBu})]** (Figure 2) and its one-electron oxidized product, which was characterized as a rare temperature persistent high valent tetracoordinated Ni^{III} complex.[34] This was in contrast with the salen derivatives for which one-electron oxidation led to a radical complex.[13, 26, 35]

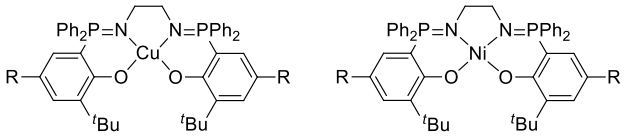

R = ^{t}Bu: **[Cu(Psalen^{tBu})]**
R = OMe: **[Cu(Psalen^{OMe})]**

R = ^{t}Bu: **[Ni(Psalen^{tBu})]**
R = OMe: **[Ni(Psalen^{OMe})]**

Figure 2. Structures of phosphasalen copper and nickel complexes studied in this work.

In the present work, we report the experimental and theoretical electronic structure studies of a series of nickel and copper complexes with two different phosphasalen ligands, the **Psalen^{tBu}** and the **Psalen^{OMe}** ligands (Figure 2). Since Ni and Cu sit next to each other in the periodic table and the geometry of the complexes is similar, a direct electronic comparison has allowed the evaluation of the metallic contribution in the overall redox delocalization in these molecules using different spectroscopies complemented by quantum chemical calculations. Several contradictions appear in the description of the electronic structure of these complexes, leading us to propose a multi-configurational ground state for these cationic copper and nickel phosphasalen complexes. This therefore represents another important contribution to the vigorous debate concerning high oxidation states.[17, 31b, 36]

Results

Synthesis and solid state studies

Synthesis

The two phosphasalen ligands (**Psalen^{tBu}**[32b] and **Psalen^{OMe}**[37]) as well as the **[Ni(Psalen^{tBu})]** and **[Ni(Psalen^{tBu})](SbF$_6$)**[34] were synthesized as previously published. In a general procedure, the phosphasalen ligand was generated *in situ* by deprotonation of the bis-aminophosphonium derivatives with potassium hydride (KH) or potassium hexamethyldisilazane (KHMDS) in THF before the addition of the metal precursor ([NiBr$_2$(DME)] or CuBr$_2$). Removal of insoluble salts by filtration of THF and CH_2Cl_2 solutions, followed by precipitation with petroleum ether, delivered the neutral complexes **[Ni(Psalen^{OMe})]**, **[Cu(Psalen^{tBu})]** and **[Cu(Psalen^{OMe})]** in 85, 66 and 82% yield, respectively. X-ray suitable crystals were obtained for all three complexes. Their structures are shown in Figures S2-4, while metric parameters are given in Tables S1, S2, S3.

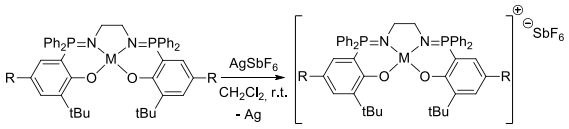

R= ^{t}Bu, OMe
M = Cu, Ni

[Cu(Psalen^{tBu})](SbF$_6$), 85 %(M = Cu, R= ^{t}Bu)
[Cu(Psalen^{OMe})](SbF$_6$), 84% (M = Cu, R= OMe)
[Ni(Psalen^{OMe})](SbF$_6$), 82% (M = Ni, R= OMe)

Scheme 1. Chemical oxidation to **[Ni(Psalen^{OMe})](SbF$_6$)**, **[Cu(Psalen^{tBu})](SbF$_6$)** and **[Cu(Psalen^{OMe})](SbF$_6$)**.

The oxidation of the neutral complexes was performed using a stoichiometric amount of silver salt ($AgSbF_6$) in order to form the ionic pairs of **[Ni(Psalen^{OMe})](SbF$_6$)**, **[Cu(Psalen^{tBu})](SbF$_6$)** and **[Cu(Psalen^{OMe})](SbF$_6$)** (Scheme 1). During the oxidation reaction, metallic silver precipitated and the color of the copper solutions changed from green to purple, while the solution of **[Ni(Psalen^{OMe})](SbF$_6$)** is dark brown. After removal of silver, the respective complexes were isolated in good yields (82 to 85 %). Recrystallized material suitable for X-ray crystallography and spectroscopic analysis were obtained from concentrated CH_2Cl_2/toluene solutions stored at -40 °C for the copper complexes, while **[Ni(Psalen^{OMe})](SbF$_6$)** was recrystallized by slow diffusion of petroleum ether into a saturated CH_2Cl_2 solution. The X-ray structure of **[Ni(Psalen^{OMe})](SbF$_6$)**, **[Cu(Psalen^{tBu})](SbF$_6$)** and **[Cu(Psalen^{OMe})](SbF$_6$)** are shown in Figures 3 and 4. Metric parameters are reported in Tables 1 and 2.

X-ray diffraction studies

Given the non-coordinating nature of hexafluoroantimonate counter anion (SbF_6^-), direct comparisons between neutral and oxidized forms are possible.

In **[Ni(Psalen^{OMe})]**, the nickel ion adopts a distorted square-planar geometry with a NOON torsion angle of 12.0 ° (Figure S2). This torsion angle is larger than the one found in **[Ni(Psalen^{tBu})]** (6.2 °). This can be further evidenced using the τ_4 parameter, which is an index of the distortion from square planar (τ_4 = 0) to tetrahedral geometry (τ_4 = 1).[38] The deviation from planarity increases by replacing one *tert*-butyl group by a methoxy one (from 0.06 to 0.12, Table 1).

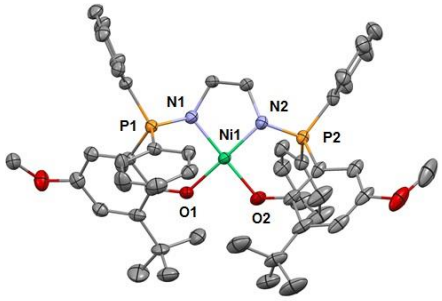

Figure 3. ORTEP of **[Ni(Psalen^{OMe})](SbF$_6$)** with thermal ellipsoids at 50 % probability. Hydrogen atoms and the SbF_6 anion have been omitted for clarity. Selected angles (deg): N1-Cu-O2 170.41(1), N2-Cu-O1 165.46(1).

Table 1. Selected bond lengths and angles for neutral and cationic nickel complexes (data for Psalen^{tBu} complexes from reference 34).

	[Ni(Psalen^{tBu})]	[Ni(Psalen^{tBu})]$^+$	[Ni(Psalen^{OMe})]	[Ni(Psalen^{OMe})]$^+$
Ni-O1[a]	1.878(1)[c]	1.828(2)	1.880(2)	1.829(3)
Ni-O2[a]	1.878(1)[c]	1.844(2)	1.885(2)	1.864(3)
Ni-N1[a]	1.888(2)[c]	1.875(3)	1.877(2)	1.874(3)
Ni-N2[a]	1.888(2)[c]	1.842(3)	1.884(2)	1.841(3)
P1-N1[a]	1.619(2)[c]	1.639(3)	1.603(2)	1.627(3)
P2-N2[a]	1.619(2)[c]	1.650(3)	1.606(2)	1.632(3)
τ_4	0.06	0.12	0.12	0.17
Torsion angle[b]	6.15	11.47	11.96	16.02

[a] in Å; [b] ($N_1O_1O_2N_2$) torsion angle in degree (°); [c] equivalent by symmetry

In both neutral complexes, the Ni-N and Ni-O bond distances are similar and shorten upon oxidation (see Table 1). The contraction is more pronounced for the Ni-O bonds which are reduced by 0.051 and 0.021 Å in **[Ni(Psalen^{OMe})](SbF$_6$)** (Figure 3). This non-symmetric contraction is also observed in the Ni-N bonds, which varies by 0.003 and 0.043 Å. As a consequence, a long axis appears along the N1-Ni-O2 segment. This contraction is accompanied by an elongation of the P-N bonds by about 0.025 Å, translating the increased donation of the iminophosphorane moieties to the metal. Similar variations were already observed for **[Ni(Psalen^{tBu})](SbF$_6$)**.[34] As found in the neutral complexes, the NOON torsion angle is larger in **[Ni(Psalen^{OMe})](SbF$_6$)** (16.0 ° compared to 11.5 ° in **[Ni(Psalen^{tBu})](SbF$_6$)**). The comparison of τ_4 shows the amplification of the distortion upon oxidation (Table 1). No quinoid pattern of the phenoxy rings is observed unlike what was reported for several oxidized **[Ni(Salen)]$^+$** complexes, in which a phenoxyl radical is formed.[13] In agreement with this observation, the O-C_{Ar} bond distances of the cationic complexes are similar to those of the neutral complexes. This indicates either the absence of a phenoxyl radical or its strong delocalization.

Thus, as for **[Ni(Psalen^{tBu})](SbF$_6$)**, the data point to a metal centered oxidation for **[Ni(Psalen^{OMe})](SbF$_6$)**.
Both **[Cu(Psalen^{tBu})]** and **[Cu(Psalen^{OMe})]** complexes display a distorted square planar geometry around the metal center (see Figure S3 and S4). The coordination bond distances are longer than those found in the analogous nickel complexes (average of 0.04 Å for the M-O distances and 0.06 Å for the M-N distances).

Table 2. Selected bond lengths and angles for neutral and cationic copper complexes.

	[Cu(Psalen^{tBu})]	[Cu(Psalen^{tBu})]$^+$	[Cu(Psalen^{OMe})]	[Cu(Psalen^{OMe})]$^+$
Ni-O1[a]	1.917(2)[c]	1.861(3)	1.923(2)	1.904(3)
Ni-O2[a]	1.917(2)[c]	1.860(3)	1.919(2)	1.882(3)
Ni-N1[a]	1.951(2)[c]	1.889(4)	1.948(2)	1.920(4)
Ni-N2 [a]	1.951(2)[c]	1.889(3)	1.941(2)	1.913(4)
P1-N1[a]	1.602(2)[c]	1.644(4)	1.597(2)	1.639(4)
P2-N2[a]	1.602(2)[c]	1.657(4)	1.593(2)	1.621(4)
τ_4	0.14	0.02	0.21	0.03
Torsion angle[b]	13.02	1.01	19.40	1.87

[a] in Å; [b] ($N_1O_1O_2N_2$) torsion angle in degree (°); [c] equivalent by symmetry

The distortion with respect to the square planar geometry is easily remarkable with a τ_4 index at 0.14 and 0.21 for **[Cu(Psalen^{tBu})]** and **[Cu(Psalen^{OMe})]** respectively. Upon oxidation an important gain in planarity is observed; the NOON torsion angle of the main plane decreases from 13.0 to 1.0° in the case of **[Cu(Psalen^{tBu})](SbF$_6$)**, and from 19.4 ° to 1.9 ° for **[Cu(Psalen^{OMe})](SbF$_6$)** (Figure 4, Table 2). The planarity is almost similar in both oxidized complexes with τ_4 values at 0.02 and 0.03. A contraction around the metal center is also observed. This contraction is more pronounced for **[Cu(Psalen^{tBu})](SbF$_6$)** where Cu-O and Cu-N bonds shorten by an average of 0.057 Å and 0.062 Å, respectively, compared to an average of 0.028 Å for both bonds in **[Cu(Psalen^{OMe})](SbF$_6$)**. In comparison with the nickel complexes, the contraction is only slightly unsymmetrical so that no shorter or longer axis forms. As previously mentioned, an elongation of the P-N bonds is also observed. The phenoxy rings and the C-OAr bonds also do not experience significant variations, as they would in the case of a radical localized on the ligand. This contrasts with the **[M(1,2-salcn^{OMe})]** (M = Cu, Ni) or **[Ni(salen^{tBu})]** complexes, in which a clear differentiation in the metric parameters is observed when either the ligand or the metal is oxidized.[12-13, 35b] In **[Cu(Psalen^{tBu})](SbF$_6$)**, the observed metric parameters are in good agreement with those found in the characterization of **[Cu(1,2-salcn^{tBu})](SbF$_6$)**,[12] which was described as a Cu^{III} complex in the solid state. These data seem to point toward a metal centered oxidation, but must be taken cautiously. In **[Cu(Psalen^{OMe})](SbF$_6$)**, even if the gain in planarity and the contraction of the coordination sphere are in favor of a Cu^{III} center, the differences observed relative to **[Cu(Psalen^{tBu})](SbF$_6$)** and in particular the weaker contraction may suggest an intermediate situation in which both ligand and the metal are getting partially oxidized. A definitive conclusion regarding the electronic structure cannot be drawn based only on X-ray structures, thus the magnetic properties of the complexes were investingated.

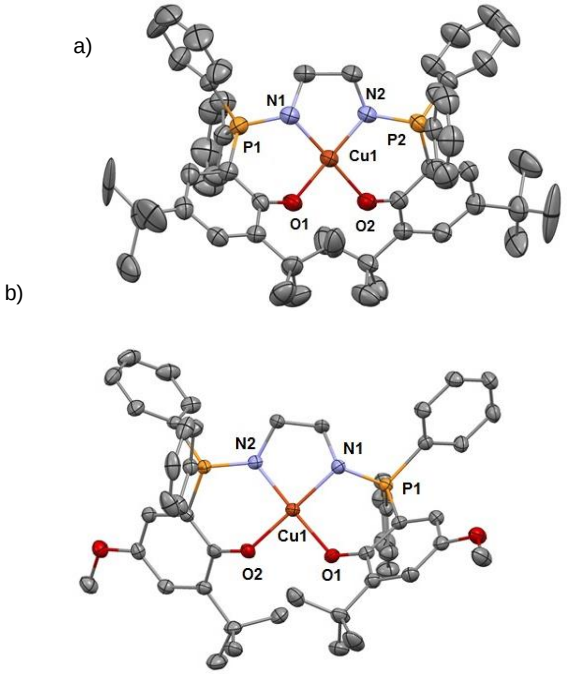

Figure 4. ORTEPs of **[Cu(Psalen^{tBu})](SbF$_6$)** (a) and **[Cu(Psalen^{OMe})](SbF$_6$)** (b) with thermal ellipsoids at 50 % probability. The SbF_6^- anion, hydrogen atoms and solvent molecules have been omitted for clarity. Selected bond angles (deg): for **[Cu(Psalen^{tBu})](SbF$_6$)**: N1-Cu-O2 178.72(1), N2-Cu-O1 178.94(2); for **[Cu(Psalen^{OMe})](SbF$_6$)**: N1-Cu-O2 178.66(2), N2-Cu-O1 177.55(2)

Magnetic studies

All complexes, except **[Ni(Psalen^{OMe})]**, were investigated over the 5-300 K temperature range. The **[Ni(Psalen^{tBu})](SbF$_6$)** complex was already measured in a previous study,[34] and showed the typical Curie behavior of a d^7 square-planar complex (C = 0.46 cm^3 K mol^{-1}) with a measured g_{iso} value of 2.22, in good agreement with typical unquenched orbital moment of a first row late transition metal. Accordingly, if **[Ni(Psalen^{OMe})]** is diamagnetic in agreement with d^8 square-planar complexes, **[Ni(Psalen^{OMe})](SbF$_6$)** shows a behavior very similar to that of **[Ni(Psalen^{tBu})](SbF$_6$)** with a χT value of 0.427 cm^3 K mol^{-1} at room temperature (see Figure S8). The g_{iso} value obtained is 2.16, slightly lower than that of **[Ni(Psalen^{tBu})](SbF$_6$)**. The measured values are indicative on an orbital contribution, which is due to a significant metallic character of the magnetic orbital. The observed slight decrease of g values between the two complexes can be interpreted by a decrease in the metal character.[35a] However, at this stage, it is wise to remember that the quantification of the ligand and metal character with this sole set of data remains dubious.

The temperature magnetic data of **[Cu(Psalen^{tBu})]** and **[Cu(Psalen^{OMe})]** are in good agreement with d^9 complexes with room temperature values of χT of 0.446 and 0.424 cm^3 K mol^{-1}, respectively (Figures S9 and S10).

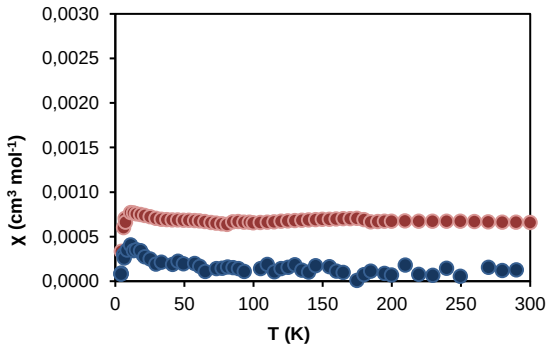

Figure 5. Temperature dependent magnetic data of **[Cu(Psalen^{tBu})](SbF$_6$)** (blue circles) and **[Cu(Psalen^{OMe})](SbF$_6$)** (red circles).

The magnetic data for **[Cu(Psalen^{tBu})](SbF$_6$)** and **[Cu(Psalen^{OMe})](SbF$_6$)** are reported in Figure 5. In both cases, the magnetic susceptibility is independent of the temperature. **[Cu(Psalen^{OMe})](SbF$_6$)** exhibits a χ value of 0.00070(5) cm^3 mol^{-1} while **[Cu(Psalen^{tBu})](SbF$_6$)** has a χ value ≈ 0.0001(1) cm^3 mol^{-1}. Both values are low but positive which indicates a temperature independent paramagnetic (TIP)[39] behavior albeit the χ value is more than seven times higher in **[Cu(Psalen^{OMe})](SbF$_6$)** than in **[Cu(Psalen^{tBu})](SbF$_6$)**. In these cases, the purity of the sample was corrected for magnetic impurities,[40] and the nature of the sample containment was chosen according to previous reports (See SI for details).[41] The observation of this TIP behavior over the large temperature range indicates that the triplet state is not populated -or to a very small extent- at room temperature and this is in favor of a relative large gap (–2*J*) between the open-shell singlet and the triplet states (above 1000 cm^{-1}). Indeed, a Boltzmann distribution over the two states, a singlet ground state and a triplet excited state, separated by 1000 cm^{-1} leads to a population of only 1 % of the triplet state at room temperature. A fit of the χT curve, which is linear over this temperature range, with an exchange coupling Hamiltonian is therefore uninformative.[17b] This is in good agreement with recent observations made by Nocera and co-workers on copper corroles[17b] and is also reminiscent to the electronic ground state of the galactose oxidase.[42]
The very low value of χ for **[Cu(Psalen^{tBu})](SbF$_6$)** has to be taken cautiously since the error is rather large and it is preferable at this stage to avoid drawing any conclusions.

Solution properties

Cyclic voltammetry

Cyclic voltammetry (CV) experiments have been performed on **[Cu(Psalen^{tBu})]**, **[Cu(Psalen^{OMe})]**, as well as **[Ni(Psalen^{OMe})]**, that can be directly compared with **[Ni(Psalen^{tBu})]**, already published.[34] The dianionic ligands have also been studied with this method as their potassium salt form (**K$_2$Psalen^{tBu}, K$_2$Psalen^{OMe}**). All the redox potentials reported and discussed in this work are expressed versus the Fc^+/Fc reference couple.
Substitution of ^{t}Bu groups by MeO groups induces a rather small change in the electronics of the ligands. Figure S11 shows the two non-reversible oxidations that are attributed to the oxidation of both phenoxide rings. Under our experimental conditions, these waves are not reversible and are indicative of the fast chemical degradation of the radical anion and the dianion that are formed in our CV experiments.

Table 3. Oxidation potentials for free ligands in V versus Fc^+/Fc in CH_2Cl_2 (0.12 M $TBAPF_6$, scan rate 0.1 V/s).

	E_{apI}	E_{apII}	$\Delta E_{I/II}$
K$_2$Psalen^{tBu} [a]	-0.15	0.15	0.30
K$_2$Psalen^{OMe} [b]	-0.33	-0.07	0.26
Δ(Psalen^{tBu}/ Psalen^{OMe})	0.18	0.22	0.04
H$_2$Salen^{tBu} [c]	0.35	0.46	0.11

[a] c = 1.5 mM; [b] c = 2.5 mM; [c] ref [43]

Results gathered in Table 3 show that the presence of the electron donating methoxy groups facilitates the first and second oxidations by 0.18 and 0.22 V, respectively, in agreement with their Hammet constant.[44] The gap between the two oxidation processes is comparable for both phosphasalen ligands (0.30 and 0.26 V) and is larger than that measured for H$_2$Salen^{tBu} in its neutral form (0.11 V).[43]

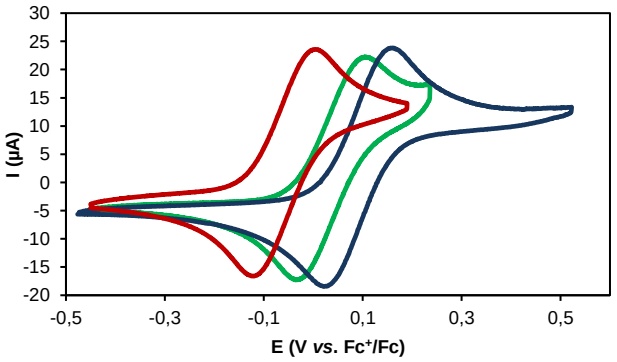

Figure 6. Cyclic voltammetry curves of the first oxidation of [Cu(Psalen^{tBu})] (blue), [Cu(Psalen^{OMe})] (green) and [Ni(Psalen^{OMe})] (red) in CH_2Cl_2 (containing 0.12 M $TBAPF_6$ and 3 mM of complex, scan rate 0.1 $V.s^{-1}$) at a carbon electrode.

The CV of **[Ni(Psalen^{tBu})]** exhibits three oxidation waves at 0.01 V (I), 0.82 V (II) and 1.24 V (III).[34] Similarly, **[Ni(Psalen^{OMe})]** exhibits three oxidation waves: a reversible one at -0.06 V (I), a pseudo-reversible at 0.47 V (II) and an irreversible one at 1.00 V (III) (see Figures 6 and S12). The three oxidations account for the possibility of oxidizing both phenoxide rings and the metal center. The first oxidation of **[Ni(Psalen^{OMe})]** is easier by 0.07 V, compared to that of **[Ni(Psalen^{tBu})]** (Figures 6 and S12, Table 4).

This is lower compared to the values measured for the free ligands (0.18 V).The striking point in these values is the gap between the first and second oxidation ($\Delta E_{I/II}$) which is 0.81 and 0.53 V in **[Ni(Psalen^{tBu})]** and **[Ni(Psalen^{OMe})]**, respectively. They strongly differ from the $\Delta E_{I/II}$ of the free ligands (0.30 and 0.26 V). Comparatively, for salen derivatives such as **[Ni(salen^{tBu})]**,[45] the first oxidation occurs at 0.59 V, and the separation between first and second oxidation $\Delta E_{I/II}$ is 0.46 V, lower to what we report here. In this complex, the two first oxidations are attributed to the oxidation of the two phenoxide groups.[45] The fact that the first oxidation is at higher potential in salen derivatives is explained by the better electron-donating ability of iminophosphoranes.

Table 4. Redox potentials for nickel and copper complexes expressed in V versus Fc^+/Fc in CH_2Cl_2 (3 mM complex, 0.12 M $TBAPF_6$, scan rate 0.1 V/s).

Compound	$E^{I}_{1/2}$	$E^{II}_{1/2}$	$\Delta E_{I/II}$
[Ni(Psalen^{tBu})]	0.01	0.82	0.81
[Ni(Psalen^{OMe})]	-0.06	0.47	0.53
[Ni(salen^{tBu})][a]	0.59	1.05	0.46
[Ni(salen^{OMe})]	-0.06	0.47	0.53
[Ni(1,2-salcn^{OMe})][b]	0.22	0.64	0.42
[Cu(Psalen^{tBu})]	0.10	0.95	0.85
[Cu(Psalen^{OMe})]	0.04	0.54	0.50
[Cu(salen^{tBu})][c]	0.55	0.75	0.20
[Cu(1,2-salcn^{OMe})][b]	0.28	0.44	0.16

[a] ref. 45; [b] ref. 13; [c] ref. 43.

[Cu(Psalen^{tBu})] and **[Cu(Psalen^{OMe})]** redox potentials are slightly shifted to anodic potentials compared to the nickel analogues (Table 4). These slight differences account for the small variation in electronegativity between both metals.[46] The first oxidation processes are mono-electronic and can be attributed to the oxidation of the metal center and/or to the phenoxide rings as described above for the nickel derivatives. The easier oxidation of **[Cu(Psalen^{OMe})]** compared to **[Cu(Psalen^{tBu})]** (ΔE = 0.06 V) is due to the methoxy substitution. The difference is noticeably smaller compared to that in the free ligands (ΔE = 0.18 V) but comparable to that of the nickel complexes (ΔE = 0.07 V). The replacement of the imines by iminophosphoranes moieties also provides easier oxidation compared to analogous salen derivatives with values of first oxidation potential of 0.55 V for **[Cu(1,2-salen^{tBu})]**[43] and 0.28 V for **[Cu(1,2-salcn^{OMe})]**.[12] Interestingly, the $\Delta E_{I/II}$ in both copper and nickel complexes is comparable for a given ligand: 0.85 V and 0.81 V, respectively, for the **Psalen^{tBu}** ligand and 0.50 V and 0.53 V, respectively, for the **Psalen^{OMe}** ligand.

The gap between the first and the second oxidation is related to the electronic structure of the one-electron oxidized species. If only the ligand is involved, the gap with the second oxidation is small. If both the metal and the ligand participate, allowing delocalization, this gap becomes larger evidencing the greater difficulty to doubly oxidize the complex because of the presence of a highly electropositive metal center. This is the case in **[Ni(salen^{tBu})]** ($\Delta E_{I/II}$ = 0.40 V),[45] to a larger extent in **[Ni(Psalen^{OMe})]** ($\Delta E_{I/II}$ = 0.53 V), and even more in **[Ni(Psalen^{tBu})]** ($\Delta E_{I/II}$ = 0.81 V).[34] From these observations, the reduced gap observed in **[Ni(Psalen^{OMe})]** compared to **[Ni(Psalen^{tBu})]** would suggest a larger contribution of the ligand in the mono-oxidized species **[Ni(Psalen^{OMe})](SbF$_6$)**. The third oxidation observed for nickel complexes reinforces this picture: $\Delta E_{II/III}$ is 0.26 V in **[Ni(Psalen^{tBu})]** and is close to the separation observed in the free ligand ($\Delta E_{I/II}$ = 0.30 V), while $\Delta E_{II/III}$ is 0.54 V in **[Ni(Psalen^{OMe})]**. The gap between the two first oxidations evolves similarly in the copper series from 0.16 and 0.20 V for **[Cu(1,2-salcn^{OMe})]** and **[Cu(salen^{tBu})],** to 0.50 and 0.85 V for **[Cu(Psalen^{OMe})]** and **[Cu(Psalen^{tBu})]** pointing also towards a stronger metallic contribution in presence of the **Psalen^{tBu}** ligand. This means that both the ligand and the metal contribution are similar in the copper and nickel complexes when they possess the same Psalen ligand.

UV-Visible spectroscopy

The spectra of neutral nickel and copper complexes and significant bands are shown in Figure S13 and Table S4. Upon oxidation, the spectra of the both copper complexes change significantly (Figure 7). They exhibit an intense band around 560 nm and a large band in the NIR region. The transition around 400 nm increases and is red-shifted to 450 nm.

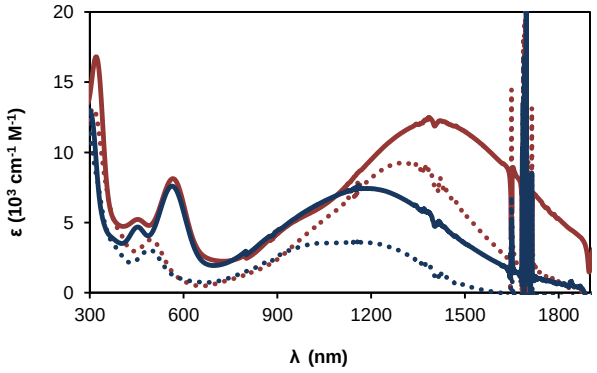

Figure 7. UV-vis spectra of **[Cu(Psalen^{tBu})](SbF$_6$)** (blue solid line) **[Cu(Psalen^{OMe})](SbF$_6$)** (red solid line), **[Ni(Psalen^{tBu})](SbF$_6$)** (blue dashed line), and **[Ni(Psalen^{OMe})](SbF$_6$)** (red dashed line) in CH_2Cl_2 at 298 K

The electronic spectrum of **[Ni(Psalen^{OMe})]** is also similar to the one described for **[Ni(Psalen^{tBu})]**.[34] This is the same for the oxidized complexes, showing a transition at 510 nm (ε = 2500 M^{-1} cm^{-1}, Figure 7), which should correspond to LMCT (Ligand to Metal Charge Transfer) as already suggested for **[Ni(Psalen^{tBu})](SbF$_6$)**. In the NIR region, all the four oxidized complexes display an intense broad band, but some slight differences are observed. **Psalen^{tBu}** complexes present less intense and blue-shifted absorptions. For **[Ni(Psalen^{tBu})](SbF$_6$)** the band is centered at 1100 nm (ε = 3600 cm^{-1} M^{-1}) and present

a $\Delta v_{1/2}$ of 550 nm. The band of **[Ni(Psalen^{OMe})](SbF$_6$)** is red-shifted to 1300 nm and its intensity increases (ε = 9200 cm^{-1} M^{-1}, $\Delta v_{1/2}$ = 520 nm). Compared to their salen analogues, the bands are blue-shifted and notably less intense. Thus **[Ni(salen^{tBu})]**, which was characterized as a fully delocalized Robin-Day class III mixed-valence complex[47] gives a large signal centered around 2130 nm (ε = 21400 cm^{-1} M^{-1}). For **[Ni(1,2-salcn^{OMe})]** several transitions were observed above 1500 nm and this complex was characterized as an intermediate class II/class III mixed-valence complex[48] For copper, as for nickel complexes, the intense band observed in the NIR region is red-shifted and more intense for the **Psalen^{OMe}** complex compared to the **Psalen^{tBu}** one: the center of the band moves from 1180 nm (ε = 7400 cm^{-1} M^{-1}, $\Delta v_{1/2}$ = 620 nm) to 1400 nm (ε = 7400 cm^{-1} M^{-1}, $\Delta v_{1/2}$ = 620 nm). The NIR spectrum of **[Cu(Psalen^{tBu})]$^+$** resembles to that obtained by F. Thomas et coll. for a bis-anilido complex (1280 nm, 7460 cm^{-1} M^{-1}), which was characterized as a Cu^{III} complex.[49] Interestingly, even if the NIR broad band look at first similar, some slight differences appear above 1000 nm contrary to the UV-vis domain. However, the bands are very large, and may correspond to a variety of different transitions precluding drawing any conclusion about the electronic structure of the complexes. Overall, the spectra of the oxidized Ni and Cu complexes bearing Psalen ligands are very similar and do not inform on any chemical structure differentiation unlike the electrochemical data.

This discrepancy poses question. Since it is clear from the CV studies that the two different ligands induce two different delocalization extents, it certainly indicates that the attribution of the similar bands observed in the optical spectra cannot be pure d → d or $\pi \rightarrow \pi^*$ transitions. According to the electrochemical data, a larger ligand based transition ($\pi \rightarrow \pi^*$) would have been expected for the complexes bearing the **Psalen^{OMe}** ligand. This is why the bands have been tentatively assigned to charge-transfer bands. This assignment is in good agreement with the literature[26a] and our previous assignments for the **[Ni(Psalen^{tBu})](SbF$_6$)** complex.[34] Therefore, in the case of a delocalized orbital, it is conceivable that the transition from a primarily ligand loaded orbital to a primarily empty metal orbital (LMCT) would have a similar intensity than the transition of a primarily metal loaded orbital to a primarily ligand empty orbital (MLCT). The problem that arises at this stage does not only lie on the nature of the ground state but on the nature of the excited states. In these complexes, when both the ligand and the metal are involved in the populated high-energy orbitals, the optical spectra are not useful for the quantification of the metallic (or ligand) contribution to the ground state without knowing the nature of the excited state.

NMR studies

All compounds were studied by solution ^{1}H and ^{31}P{^{1}H} NMR spectroscopy. **[Ni(Psalen^{OMe})]** and **[Ni(Psalen^{OMe})](SbF$_6$)** possess spectra similar to those reported for **[Ni(Psalen^{tBu})]** and its oxidized species.[34] **[Ni(Psalen^{OMe})]** displays a typical diamagnetic spectrum with a ^{31}P{^{1}H} resonance at 35.2 ppm, in agreement with a Ni^{II} square planar d^8 complex. **[Ni(Psalen^{OMe})](SbF$_6$)** exhibits a paramagnetic ^{1}H NMR spectrum (Figure S14) with no ^{31}P{^{1}H} NMR resonance, which may indicate a Ni^{III} square planar d^7 center. The ^{1}H NMR spectrum of **[Ni(Psalen^{OMe})](SbF$_6$)** was recorded at different temperatures (Figure S15) and agrees well with a paramagnetic complex following the Curie law. At 20 °C, the methyl resonance of the methoxy groups has a chemical shift of 33.98 ppm, the aromatic protons from the phenoxide resonate at 25.99 and -2.84 ppm, while the ^{t}Bu groups resonate at 2.88 ppm. The isotropic paramagnetic shift ($\delta^{para} = \delta^{obs} - \delta^{dia}$) is therefore 30.56 ppm for the methoxy group, 19.12 ppm for one set of the aromatic protons, 9.71 ppm for the second set and 1.52 ppm for the ^{t}Bu groups at 25 °C. For comparison, in the case of **[Ni(Psalen^{tBu})](SbF$_6$)** the paramagnetic isotropic shifts δ^{para} were 11.89 and 9.18 ppm for the two aromatic protons; and 1.14 and 1.81 ppm for the two ^{t}Bu groups. From the NMR data, it seems that **[Ni(Psalen^{OMe})](SbF$_6$)** has more pronounced isotropic shifts than **[Ni(Psalen^{tBu})](SbF$_6$)**. The paramagnetic isotropic shift has two contributions, the pseudo-contact (δ^{PC}) and the Fermi contact (δ^{FC}).[50] The former relates to the magnetic susceptibility tensor as well as the metrical parameters between the observed proton and the paramagnetic center. The latter relates to the extent of the spin density experienced by the observed protons. The geometry modifications between **[Ni(Psalen^{tBu})](SbF$_6$)** and **[Ni(Psalen^{OMe})](SbF$_6$)** are rather small but sizeable. It is therefore difficult to attribute the origin of the different isotropic shifts since both contributions (electronic and geometric) may be involved in these data. However, **[Ni(Psalen^{OMe})](SbF$_6$)** has a lower g_{iso} value but an increased isotropic shift, which is contradictory. It is therefore reasonable to consider a strong influence of the Fermi contact, *i.e.*, an increased spin density on the phenoxy ring, which dominates the observed paramagnetic isotropic shift. This agrees with a larger ligand contribution to the magnetic orbital in **[Ni(Psalen^{OMe})](SbF$_6$)** complex, *i.e.,* a larger metal contribution in **[Ni(Psalen^{tBu})](SbF$_6$)** as suggested by CV data.

For **[Cu(Psalen^{tBu})]** and **[Cu(Psalen^{OMe})]** no ^{31}P{^{1}H} NMR signal was observed as expected for paramagnetic d^9 complexes. Their ^{1}H NMR spectrum displayed broad signals, among which those corresponding to the *tert*-butyl and methoxy groups as well as one of the phenoxide protons have been assigned. **[Cu(Psalen^{tBu})](SbF$_6$)** possesses an apparent diamagnetic behavior at room temperature and a broad ^{31}P signal is present at 41.8 ppm in CD_2Cl_2 (see Figure S16). Its ^{1}H NMR spectrum exhibited six broad signals (see Figure S17) at 7.82, 7.73, 6.56, 2.95, 1.40 and 1.14 ppm which were tentatively assigned to the aromatic protons (PPh_2 and phenoxide), one phenoxide proton, the alkyl linker, and the two *tert*-butyl groups, respectively. To rule out the presence of paramagnetic species in solution the ^{1}H NMR spectrum has been recorded at different temperatures from 20 to -90 °C (see Figure S18). No significant change was observed along this temperature range, except for the resolution of one of the phenoxide protons, and the decoalescence of the signal corresponding to the ethylene bridge, which is characteristic of a rigid structure at the NMR timescale at low temperature. The absence of a significant temperature dependence tends to indicate that **[Cu(Psalen^{tBu})](SbF$_6$)** is *diamagnetic* in agreement with a square planar d^8 complex in solution. Nevertheless, SQUID

measurements point towards an open shell singlet for this complex.

The situation is different for **[Cu(Psalen^{OMe})](SbF$_6$)** which presents a broader ^{1}H spectrum than **[Cu(Psalen^{tBu})](SbF$_6$)** (Figure S19). No ^{31}P{^{1}H} NMR signal is observed at room temperature, an indication of the paramagnetic nature of the species. Two resonances were found particularly shifted compared to the typical diamagnetic shift: one at 5.65 ppm, assigned to the protons of the methoxy group, and the other at 4.65 ppm, assigned to one of the aromatic phenoxide protons. For these two resonances, the isotropic shift is calculated from the corresponding **[Ni(Psalen^{OMe})]** chemical shifts, a diamagnetic d^8 square planar analogue, and are 2.23 and 2.22 ppm for the methoxy group and the aromatic phenoxide proton, respectively. As an additional note, the paramagnetic isotropic chemical shift δ^{para} of the ^{t}Bu group is only 0.06 ppm.

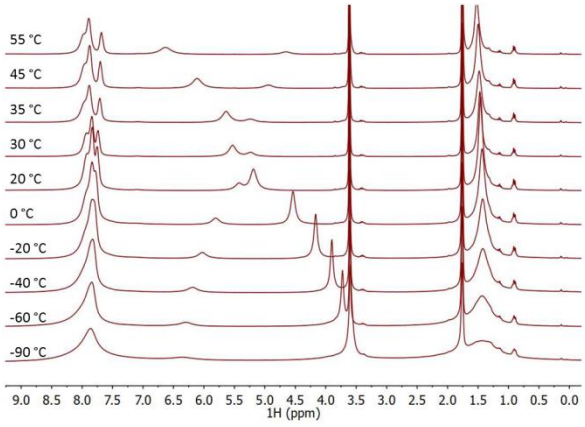

Figure 8. ^{1}H NMR spectra of **[Cu(Psalen^{OMe})](SbF$_6$)** in THF-d$_8$ at different temperatures.

The variable temperature ^{1}H and ^{31}P NMR studies, conducted in THF, are presented in Figures 8, S20 and S21. The phosphorus atoms display a broad signal around 47 ppm below -70 °C (Figure S21). From 55 to -90 °C, the proton resonances broaden with the exception of the methoxy group. The two resonances with maximum paramagnetic isotropic shift (those of methoxy and one phenoxide protons) experienced significant shifts when changing the temperature. A plot of these chemical shifts in function of the inverse of the temperature is given in Figure S22. At low temperature the paramagnetic isotropic shift δ^{para} decreases to values of 0.12 and 0.52 ppm for the methoxy and the aromatic phenoxide protons, respectively. In addition, the chemical shift variation is not linear *vs* the temperature (Figure S22). This, added to the evolution of the paramagnetic isotropic shifts with the temperature, indicates a singlet ground state and a triplet excited state that is getting partially populated at high temperatures. A fit of the chemical shift variation with the temperature is therefore possible according to the equation proposed by Le Guennic *et al*.,[51] that is derived from the Fermi contact contribution of the paramagnetic isotropic shift, here adapted to **[Cu(Psalen^{OMe})](SbF$_6$)** (Equation 1).

$$\delta(\text{ppm}) = \delta_{\text{singlet}} + 10^6 \frac{g\beta_e}{g_N\beta_N} \frac{aS(S+1)}{kT} \left[3 + \exp\left(\frac{\Delta E_{T\text{-}S}}{RT}\right)\right]^{-1} \quad (1)$$

With g, g_N being the electronic and nuclear g-values, respectively, β_e, β_N the Bohr and nuclear magnetons respectively, a the isotropic hyperfine coupling constant, S the spin of the system, k the Boltzmann constant, and R the gas constant (see SI for details).

This analysis leads to the fit of the different unknown parameters: $\delta_{singlet}$= 3.55 ppm and a_H= -1.63 G for the methoxy group and $\delta_{singlet}$= 6.38 ppm and a = 2.87 G for the phenoxide proton. The energy difference between the two states is $\Delta E_{T\text{-}S}$ = 17 kJ mol^{-1}, *i.e.*, 1420 cm^{-1} or 0.176 eV. This is in good agreement with the value obtained by Nocera and coworkers in a Cu corrole complex[17b] and indicates a large energy gap between the singlet ground state and the triplet state. The question still remains on the nature of the singlet ground state: an open-shell configuration where a strong antiferromagnetic coupling between the Cu^{II} center and the phenoxyl radical cation is present, or a closed-shell singlet, *i.e.*, a d^8 Cu^{III} complex. It is important to note that the $\delta_{singlet}$ obtained from Equation 1 are not in perfect agreement with the δ^{dia} obtained from **[Ni(Psalen^{OMe})]**. It seems that another contribution is present in the $\delta_{singlet}$ of **[Cu(Psalen^{OMe})](SbF$_6$)**, and thus the presence of an open-shell singlet is then likely, in agreement with the solid-state magnetic data.

Because of the behavior of **[Cu(Psalen^{OMe})](SbF$_6$)**, the *diamagnetism* of **[Cu(Psalen^{tBu})](SbF$_6$)** is also in question. An alternative ground state formulation could be given: an open-shell singlet ground state with a high-energy triplet above it, which cannot be substantially populated at room temperature. Increasing the temperature did not, however, allow observing any significant shift in the aromatic protons of the phenoxy group. Yet there is a contradiction for **[Cu(Psalen^{tBu})](SbF$_6$)** between the NMR and the solid state magnetic data, giving a different metallic electronic count. ^{1}H NMR studies picture a *diamagnetic* complex at room temperature without significant changes when varying the temperature, whereas the low but positive value of the magnetic susceptibility points to an open-shell singlet, S=0 (d^9,L$^{\bullet+}$) which is far below the triplet (large singlet-triplet energy gap). These contradictions suggest that [**Cu(Psalen^{tBu})](SbF$_6$)** complex has relative contributions of both the open-shell and the closed-shell singlet, *i.e.* a multi-configurational ground state.

EPR studies

X-band EPR spectra were recorded for all paramagnetic compounds: **[Ni(Psalen^{OMe})](SbF$_6$)**, **[Cu(Psalen^{tBu})]**, **[Cu(Psalen^{OMe})]**, **[Cu(Psalen^{tBu})](SbF$_6$)** and **[Cu(Psalen^{OMe})](SbF$_6$)** (Figures S23-27). Dichloromethane solutions of **[Cu(Psalen^{tBu})]** (Figure S23) and **[Cu(Psalen^{OMe})]** (Figure S24) were recorded at room temperature and show typical EPR spectra for d^9 copper complexes in a rhombic environment (g_1 = 2.124, g_2 = 2.107, g_3 = 2.051) with hyperfine coupling constants A_{Cu} of 251, 210 and 90 MHz for **[Cu(Psalen^{tBu})]** and of 251, 210 and 75 MHz (g_1 = 2.122, g_2 = 2.105, g_3 = 2.051) for **[Cu(Psalen^{OMe})]** (see Table S5). A superhyperfine coupling with the two nitrogen atoms is also observed, with A_N of 28 MHz for both complexes. This value is in agreement with those found in

the case of copper salen or corrole complexes.[17b, 52] Both spectra are very similar despite the replacement of a ^{t}Bu group by a methoxy group. **[Cu(Psalen^{tBu})](SbF$_6$)** and **[Cu(Psalen^{OMe})](SbF$_6$)** have been found to be both EPR silent over the studied temperature range (77 K to room temperature) in perpendicular mode. This reinforces the presence of a singlet ground state in both cases.

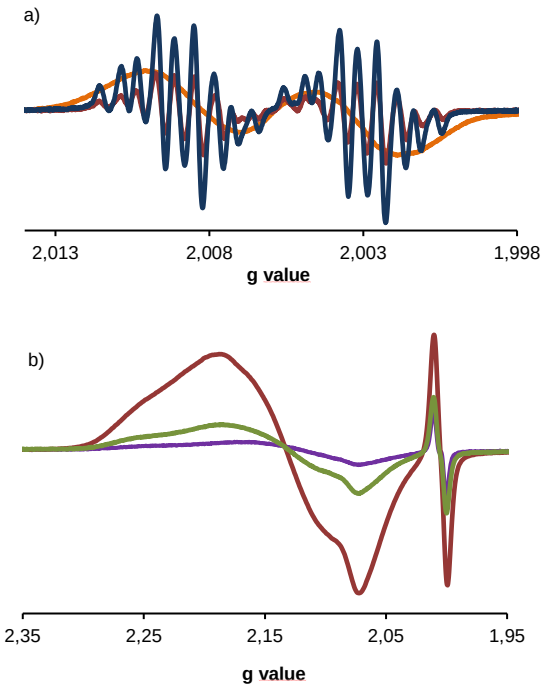

Figure 9. X- band EPR spectra of **[Ni(Psalen^{OMe})](SbF$_6$)** in CH_2Cl_2 at (a) 220 K (blue line), 180 K (red line) and 140 K (orange line) (b) 10 K (red line), 40 K (green line) and 80 K (purple line).

The EPR spectrum of **[Ni(Psalen^{tBu})](SbF$_6$)** showed no signal at room temperature, and a rhombic signal typical of a d^7 metal center[34] at low temperature. This behavior is explained by fast relaxation allowed by low-lying spin orbit states.[53] The spectrum of **[Ni(Psalen^{OMe})](SbF$_6$)** (Figure 9) is rather unusual. Contrary to **[Ni(Psalen^{tBu})](SbF$_6$)**,[34] the spectrum at room temperature exhibits an isotropic, narrow and complicated pattern centered at g_{iso} = 2.005, in agreement with the typical spectrum of organic radical species (Figure S27). At first glance, the spectrum is composed of two main transitions that are split in about ten bands (9-10 G), although their number is difficult to assess because of overlaps. The simulation of this spectrum (Figure S27) was made taking into account both the aromatic protons from the phenoxide ring (A_H = 25.83 MHz, 1H and A_H = 2.01 MHz, 1H) and the methyl protons of the ^{t}Bu group (A_H = 3.08 MHz, 9H). The protons of the methoxy group were not used in this simulation, which contrasts with the VT-NMR results. This can be explained by a less efficient hyperconjugation mechanism to transfer the spin density on the methyl proton of the methoxy group compared to the ^{t}Bu group. With a decrease of the temperature the spectrum broadens, a common feature in organic radicals,[54] to yield a broad doublet at 140 K (Figure 9a, orange line). Below 100 K, a new feature appears at low field, while the doublet continues to broaden before finally coalescing (Figure 9b). The new feature is composed of three transitions in good agreement with a Ni^{III} d^7 rhombic structure. A similar behavior was observed for **[Ni(Psalen^{tBu})](SbF$_6$)** albeit no radical signal was present.[34] The rhombic g matrix was simulated with g values of 2.07, 2.15 and 2.21 (g_{av} = 2.14) while the isotropic radical signal is centered at g_{iso} = 2.005 (Figure S26, Table S6). The ratio between the two signals was not investigated because of the fast relaxation of the metallic signal at high temperature and the saturation of the radical at low temperature. The rhombic g matrix of the Ni^{III} center is somewhat different to that of **[Ni(Psalen^{tBu})](SbF$_6$)** with a lower g_{av} value (2.14 *vs*. 2.19). This fits with the magnetic data, in which a g_{iso} value of 2.16 was measured. In agreement with the solid-state X-ray data, the xy plane defined by the NOON coordination environment is not strictly planar and one of the axes is significantly shortened; the signal has therefore a rhombic symmetry. Additionally, the solid-state EPR data of **[Ni(Psalen^{OMe})](SbF$_6$)** do not show a ligand feature but only a rhombic g matrix (Figure S25) which agrees with a Ni^{III} formulation. Differentiation of the electronic structure between solid-state and solution have already been reported[12] and shed light on the subtle bias that this ligand backbone offers upon variation of the phenoxide substituents.

The behavior of **[Ni(Psalen^{OMe})](SbF$_6$)** may be interpreted in different manners: i) an incomplete temperature-induced valence tautomerism where an electron shifts from the metal (at high temperatures) towards the ligand (at low temperatures); ii) a delocalized orbital (metal and ligand character) allowing both signals to appear at low temperature; and iii) a multi-configurational electronic structure with several different configurations: some with a ligand radical, others with the oxidized metal. The eventuality of an incomplete valence tautomerism cannot be ruled out since the solid-state and solution EPR data are different. However, the effective magnetic moment was measured in solution with the Evans' method and a value of 1.9 μ_B was obtained at room temperature. This is higher than the theoretical effective magnetic moment of a radical species and may indicate an orbital contribution to this moment. This seems to disprove the valence tautomerism hypothesis. Therefore, it is conceivable that the EPR data of the **[Ni(Psalen^{OMe})](SbF$_6$)** complex suggest a multi-configurational ground state, in which the wave function is composed of a primary ligand magnetic orbital and a primary metallic magnetic orbital. This was also suggested for the oxidized copper complexes after solid-state and VT-NMR studies.

Theoretical studies

DFT geometries and electronic structures

All complexes have been studied by DFT in order to accurately reproduce the geometry. The TPSSh functional was first selected for its accurate description of spin states in transition metal

complexes as it was shown in various DFT studies.[55] Furthermore, TPSSh was associated to the D3 approach to include explicitly dispersion effects[56] in such complexes exhibiting bulky ligands. Most importantly, TPSSh-D3 was found to be the best compromise to reproduce the experimental trends for the changes in geometry upon oxidation. The DFT bond length changes correlate well with the X-ray values (Table S7-10). However, the Cu^{II} complexes are predicted to be more planar with smaller NOON torsion angle values than experimentally observed. The electronic structure of the eight complexes has been computed at the TPSSh-D3/ZORA/TZ2P level (Figure S28). In the four neutral species, the highest occupied molecular orbital (HOMO) has a similar shape with a strong metal character and a delocalization on the phenoxide rings. Upon oxidation, this mixed metal-ligand character remains for the HOMO with no significant difference between the cationic complexes. It is difficult to provide a more detailed description from the DFT analysis; we therefore turned to multi-referential methods.

CASSCF calculations

For both oxidized nickel complexes, state-average CASSCF calculations have been carried out with a doublet as the requested spin. The starting orbitals were built by allowing the single electron to be in either a π-ligand or a d-Ni orbital. The resulting active molecular orbitals for which an occupation with unpaired electrons occurs are provided in Figures 11 and 12.

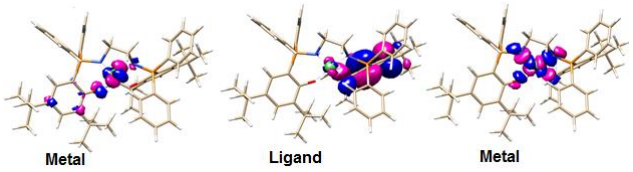

Figure 10. Active space molecular orbitals occupied by unpaired electrons associated to their "metal" or "ligand" character for **[Ni(Psalen^{tBu})]$^+$**.

For **[Ni(Psalen^{tBu})]$^+$**, the ground state is mainly composed of two configurations (see Chart 1). The main one (55 %) corresponds to the unpaired electron located in a metal-type orbital. The second one (12 %) is characterized by three unpaired electrons in two metal-type orbitals and one π-ligand orbital (Figure 10). In the **[Ni(Psalen^{OMe})]$^+$** complex, the main configuration corresponds to the unpaired electron in an orbital having both metal and ligand character (weight of 41 %). Two other configurations have a significant weight: i) one unpaired electron in a metal-type orbital (11 %), ii) three unpaired electrons in two metal-ligand character orbitals and one metal-type orbital (9 %), (Figure 11). The CASSCF calculations show that both complexes have a multi-configurational ground state. However, **[Ni(Psalen^{tBu})]$^+$** has clearly a stronger metal character than **[Ni(Psalen^{OMe})]$^+$**, for which the ground state presents a larger spin delocalization on the ligand.

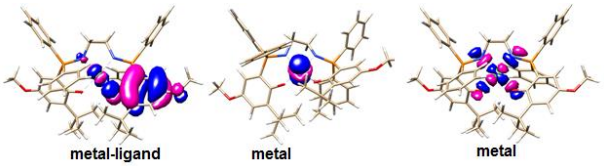

Figure 11. Active space molecular orbitals occupied by unpaired electrons associated to their "metal" or "ligand" character for **[Ni(Psalen^{OMe})]$^+$**.

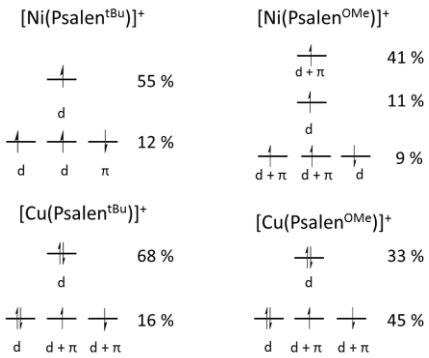

Chart 1. Electronic structure of the four oxidized complexes computed from CASSCF/TZVP state-average calculations.

This multi-configurational ground state picture agrees well with the observation of both the metal and the ligand EPR transitions at low temperature. This also relates with NMR experiments showing a stronger Fermi contact contribution for **[Ni(Psalen^{OMe})](SbF$_6$)** and with the electrochemistry data, indicative of a reduced metal character in the same complex.

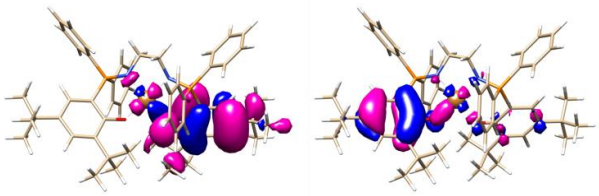

Figure 12. Active space molecular orbitals occupied by unpaired electrons with a "metal-ligand" character for **[Cu(Psalen^{tBu})]$^+$**.

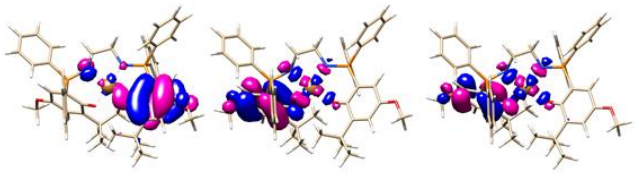

Figure 13. Active space molecular orbitals occupied by unpaired electrons with a "metal-ligand" character for **[Cu(Psalen^{OMe})]$^+$**.

For both Cu complexes, state-average CASSCF calculations have been carried out with both a singlet and a triplet as the requested spin. The triplet has been found higher in energy by 24.4 kJ/mol (2039.7 cm^{-1}) and 27.8 kJ/mol (2323.9 cm^{-1}) for **[Cu(Psalen^{tBu})]$^+$** and **[Cu(Psalen^{OMe})]$^+$** respectively.

For the singlet ground state, the active starting orbitals were built on the closed-shell SCF wave function. The resulting active molecular orbitals necessary to describe the ground states of the complexes are provided in Figures 13 and 14.

For both complexes, the ground state was found to be multi-configurational as well (see Chart 1). For **[Cu(Psalen^{tBu})]$^+$**, the main configuration corresponds to the closed-shell singlet, Cu^{III} d^8 (68 %). A second configuration with a weight of 16 % corresponds to two unpaired electrons in two metal-ligand orbitals (Figure 12). The remaining 15 % is distributed among many other configurations. The situation is slightly different in the **[Cu(Psalen^{OMe})]$^+$** case for which the closed-shell configuration has only a weight of 33 %. Two other configurations with a global weight of 45 % correspond to the two unpaired electrons located in two metal-ligand orbitals (see Figure 13 for the three occupied orbitals). The remaining 20 % is distributed among many other configurations.

As in the nickel complexes, both copper complexes possess a multi-configurational ground state with some metallic character, and a larger delocalization of the valence orbital for **[Cu(Psalen^{OMe})]$^+$**.

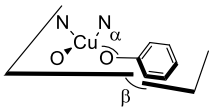

Figure 14. Schematic representation of the α and β angles.

However, the singlet state formulation does not correspond to that reported for oxidized copper salen complexes, which are generally described as ferromagnetically coupled radical complexes.[12] This may be explained by geometrical differences associated with the presence of the iminophosphorane (N=P) function.[33] The phosphorus atom is engaged in four bonds, therefore the NPC and CPC angles range between 103 and 117 ° in all complexes, indicative of a nearly tetrahedral arrangement. This contrasts with the sp^2 hybridization of the carbon in the imine group of salen complexes, and explains why the planes of the Psalen phenoxide cannot be found in the NOON coordination plane. This geometrical distortion can be measured with both the CuOC(phenoxide) angle (α angle), as well as the torsion angle between the plane of the phenoxide ring and the NOON coordination plane (β angle) (Figure 14).[57]

In all complexes, oxidized or not, the α angle ranges from 125 to 130 ° while the β angle is between 32 and 44 °, close to those found in the galactose oxidase (α = 129 ° and β = 75 °),[57] in contrast with the values of 180 and 90 ° found in copper salen complexes.[12] Thus, from a geometrical point of view, phosphasalen ligands are better structural models for the galactose oxidase, which possesses an open-shell singlet ground state (S=0). The orientation of the π orbital of the tyrosine radical with respect to the magnetic dx^2-y^2 orbital in the xy plane of the copper, *i.e.* the α and β angles, has been proposed to be the reason for such an electronic structure by Wieghardt and coworkers.[57] This is in agreement with Goodenough and Kanamori rules for singlet and triplet discrimination.[58] In phosphasalen complexes the large β angle allows large orbital overlap and covalency, therefore creating a bonding delocalized orbital, which possesses both metal and ligand character. Moreover, a slight difference in the β angle is noticeable when comparing **Psalen^{tBu}** and **Psalen^{OMe}** in our series of complexes (36 ° *vs* 44 °), probably due to a reduced steric pressure in the latter. These slight differences set up an important geometric consideration aside from the usual electronic argument in order to better explain the electronic structure of the complexes reported here. The orbital overlap is slightly greater with the **Psalen^{OMe}** than with **Psalen^{tBu}** ligand but certainly considerably larger compared to salen complexes. The formation of an open-shell singlet state in **[Cu(Psalen^{OMe})]$^+$** is allowed by the geometrical considerations (α and β angles) as observed in the galactose oxidase, whereas the **Psalen^{tBu}** ligand favors the formation of a magnetic orbital that has more metallic character. The differences observed experimentally between solid-state and solution may also account for slight modifications of the α and β angles in both phases.

The magnitude of the orbital overlap, may allow several configurations, in which the wave function is composed of a primary ligand magnetic orbital and a primary metallic magnetic orbital, to contribute to the electronic ground state of the molecule. Therefore, the eventuality of a multi-configurational ground state was considered to account for the experimental results. Despite this, the proximity of the two fragments associated to an increased orbital overlap renders the accurate description of the spectroscopic oxidation state of the copper and of the nickel metal ions rather difficult. Nevertheless, overall the model fits: both the electronics (energy difference between the two fragments) and the geometry (reduced β angle) play a role in the ratio of metal *vs* ligand spin density.

Conclusions

In summary, we synthesized four phosphasalen complexes, which differ by the nature of the metal (Ni and Cu) and/or the *para* substituent on the phenoxide (^{t}Bu *vs* OMe) and studied their mono-oxidized products to determine as accurately as possible their electronic structure. With that purpose we performed solid-state analysis (X-ray diffraction, magnetic measurements), solution studies (cyclic-voltammetry, UV-vis, NMR and EPR spectroscopies) as well as quantum chemical calculations. Both experimental and theoretical data evidenced similar electronic structure for copper and nickel complexes when bearing the same ligand. Solid-state structures of all complexes do not show a localized ligand radical, and a strong delocalization is therefore suggested. However, the phosphasalen ligand **Psalen^{tBu}** favors a magnetic orbital with more metallic character. For copper complexes, the experimental data indicate an open-shell singlet ground state with substantial contribution from a closed-shell singlet, especially with the **Psalen^{tBu}** ligand. Indeed, the magnetic measurements of **[Cu(Psalen^{tBu})](SbF$_6$)** picture a d^9 copper(II)-radical ligand complex with strong antiferromagnetic coupling (TIP behavior), while the NMR spectra agree with a *diamagnetic* d^8 copper(III) complex. Likewise, the solution EPR data for

[Ni(Psalen^{OMe})](SbF$_6$) are also surprising since both nickel(III) and nickel(II) radical forms are observed on the same spectrum. A multi-configurational ground state is proposed to account for these experimental contradictions for both copper and nickel complexes. The four complexes were studied using DFT and present a high degree of orbital delocalization, showing that all oxidized complexes are very similar at this level of theory. However, the CASSCF calculations confirm the experimental observation of multi-configurational ground states for these complexes. The main configuration found for **[Ni(Psalen^{tBu})]** shows a single electron in a metal based orbital, whereas for **[Ni(Psalen^{OMe})]** the single electron resides on a metal-ligand based orbital with a strong contribution of the phenoxide. For **[Cu(Psalen^{tBu})]**, the main configuration corresponds to a closed-shell singlet, while for **[Cu(Psalen^{OMe})]**, the ligand character is larger and the closed-shell configuration is minor (33 %) in this case. The larger ligand character, that is found for oxidized complexes featuring **Psalen^{OMe}** can be explained by the greater electron density of the phenoxide rings but also by geometrical considerations since their larger β angle allows larger interaction energy (orbital overlap). More generally this study shows how subtle changes can result in diverging properties and electronic structures while relying on a similar formalism. In phosphasalen ligands, the introduction of the phosphorus atoms offers a supplementary structural variation compared to salen derivatives, influencing both the electronics and the geometry. It would be highly interesting to study how the modifications of the substituents of this heteroatom, as well as that of the nitrogen linker, affect the electronic structure of the mono-oxidized complexes. Work in that direction is in progress in our laboratory.

Experimental Section

General considerations. All experiments were carried out under inert conditions, either under a pure nitrogen atmosphere using Schlenk technics or in a drybox (O_2 < 1 ppm, H_2O < 0.1 ppm). Anhydrous solvents were used directly from a MBraun MB-SPS 800 solvent purification machine. [$NiBr_2$(DME)][59] and bis-aminophosphonium proligands[32b, 37] were prepared according to the literature. All other reagents and deuterated solvents were obtained commercially and used without further purification. NMR spectra were recorded on a Bruker Avance 300 spectrometer operating at 300 MHz for ^{1}H, 75.5 MHz for ^{13}C and 121.5 MHz for ^{31}P. Solvent peaks were used as internal references for ^{1}H and ^{13}C chemical shifts (ppm). ^{31}P{^{1}H} chemical shifts are relative to a 85% H_3PO_4 external reference. The following abbreviations are used: br., broad; s, singlet; d, doublet; dd, doublet of doublets; t, triplet; m, multiplet.

Elemental analyses were performed by the Elemental Analysis Service of the London Metropolitan University (United Kingdom). UV-Visible spectra were recorded in the 300-1000 nm range at room temperature on an Agilent Cary 60 Spectrometer, while the NIR spectra were recorded on an Agilent Cary 5000 spectrometer in the 300-2000 nm range. In both cases 10 mm quartz cuvettes were used with solvent background correction. The Single crystals were mounted on a kapton loop using Paratone® oil and cooled to 150 K in a nitrogen stream for X-ray structure determination. All data were collected on a Nonius Kappa CCD APEXII diffractometer using Mo Kα (λ = 0.71069 Å) X-ray source and a graphite monochromator. The crystal structures were solved in SIR97,[60] SHELXL-97 and SHELXL-2014, and refined in SHELXL-97[61] and SHELXL-2014 by full-matrix least-squares using anisotropic thermal displacement parameters for all non-hydrogen atoms. Hydrogen atoms were placed either at geometrically calculated positions or according to the localization of electronic densities around the carbon atoms and refined isotropically. Cif files were deposited to the Cambridge Data Base Center under the reference CCDC numbers: 1550870 to 1550875. Details of crystal data and structure refinements are summarized in Tables S1 to S3.

Magnetic measurements were performed using a Cryogenic SX600 SQUID magnetometer. Solid samples were placed in quartz tubes under inert atmosphere. Magnetic susceptibility measurements were recorded at 5 T for **[Cu(Psalen^{OMe})](SbF$_6$)** and **[Cu(Psalen^{tBu})](SbF$_6$)**, and 0.5 T and 2 T for **[Ni(Psalen^{OMe})](SbF$_6$)**, in the 4-300 K temperature range. X-band EPR spectra were recorded on a Bruker ELEXSYS 500 spectrometer equipped with a Bruker ER4119HS X band resonator, an Oxford Instrument continuous flow ESR 900 cryostat, and a temperature control system. Samples of the oxidized complexes were prepared in the glove box using dichloromethane as solvent with some drops of toluene in quartz tubes. All spectra were recorded under non saturating conditions. Electrochemical experiments were performed using a VERSASTAT potentiostat. The counter electrode used was a Pt wire; the working electrode used was a glassy carbon electrode; and the reference electrode was a SCE. All the experiments were carried out under inert atmosphere in a 12 mL CH_2Cl_2 solution with 0.12 M tetrabutylammonium hexafluorophosphate ($TBAPF_6$) as supporting electrolyte and 3 mM complex.

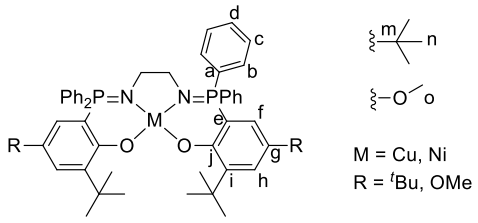

Figure 15 Labelling scheme of atoms in phosphasalen complexes.

The syntheses of **[Cu(Psalen^{tBu})]** and **[Cu(Psalen^{tBu})](SbF$_6$)** are presented below as examples, other synthetic protocols are reported in SI.

*Synthesis of **[Cu(Psalen^{tBu})]***: KHMDS (358 mg, 1.8 mmol) was added to a suspension of bis-aminophosphonium **(H$_4$Psalen^{tBu})Br$_2$** proligand (450 mg, 0.45 mmol) in 30 mL of THF. After stirring 2 h at room temperature the ^{31}P{^{1}H} NMR spectrum showed a sole singlet at 20 ppm, indicating that the deprotonation was completed. Insoluble salts were removed by centrifugation and $CuBr_2$ (100 mg, 0.45 mmol) was added into the clear solution. After 2 h of stirring, the solution turned green and no ^{31}P{^{1}H} NMR

signal was observed. The solvent was removed under reduced pressure and the residue dissolved in CH_2Cl_2 and centrifuged. The solution was concentrated and a green precipitate was obtained by addition of petroleum ether. The green solid was washed with more petroleum ether and dried under reduced pressure to yield **[Cu(Psalen^{tBu})]** (270 mg, 66 %). Crystals were obtained via evaporation of a $CDCl_3$ solution. $^{31}P\{^1H\}$ NMR ($CDCl_3$): no signal; ^1H NMR ($CDCl_3$) δ 9.38 (br. s, H_b,H_c,H_d), 6.98 (br. s, H_f,H_h), 3.34 (br. s, H_p), 1.56 (br. s, H_l or H_n), 0.99 (br. s, H_l or H_n). Anal. Calcd. for $C_{54}H_{64}Cu\ N_2O_2P_2$: C, 72.18; H, 7.18; N, 3.12; Found: C, 72.29; H, 7.30; N, 2.98. UV-vis : λ, nm (ε, $cm^{-1}\ M^{-1}$) : 625 (960), 310 (14000).

Synthesis of **[Cu(Psalen^{tBu})](SbF$_6$)** (250 mg, 0.28 mmol) was dissolved in CH_2Cl_2 (4 mL). Addition of $AgSbF_6$ (96 mg, 0.28 mmol, 1 equiv.) to the solution immediately resulted in a color change from green to deep purple together with the formation of a suspension of Ag. This suspension was stirred for 1 h and then filtered. The solvent was removed under reduced pressure and the residue dissolved in a minimum amount of diethyl ether. A purple precipitate was obtained by addition of petroleum ether and then washed with more petroleum ether (3 × 10 mL). The solid was dried under reduced pressure to obtain **[Cu(Psalen^{tBu})](SbF$_6$)** as an analytically pure purple powder (269 mg, 85 %). Dark purple crystals were obtained after one week of storage of a saturated solution of toluene/CH_2Cl_2 at -40 °C. $^{31}P\{^1H\}$ NMR (CD_2Cl_2): δ 41.8 ppm; ^1H NMR (CD_2Cl_2) δ 7.50-8.09 (m, 22H, H_b, H_c, H_d, H_h), 6.56 (br. s, 2H, H_f), 2.95 (br. s, 4H, H_p), 1.40 (br. s, 18H, H_l or H_n), 1.14 (br. s, 18H, H_l or H_n). Anal. Calcd. for $C_{54}H_{64}F_6N_2NiO_2P_2Sb$: C, 57.18; H, 5.69; N, 2.47. Found: C, 57.12; H, 5.84; N, 2.57. UV-vis: λ, nm (ε, $cm^{-1}\ M^{-1}$) : 430 (1400), 560 (7400).

Acknowledgements

We thank Dr. Isabelle Maurin (PMC, Ecole Polytechnique) for the access to the SQUID, M. Sylvain Chevalier (PMC, Ecole Polytechnique) for helping measuring NIR absorptions, Dr. Bruno Boizot (LSI, Ecole Polytechnique) for allowing the use of the LSI's EPR spectrometer. The French National Agency for research is acknowledged for funding this project (PsalenOx, JCC project n°13-JS07-0001-01), the CNRS and the Ecole polytechnique are thanked for financial support.

Keywords: electronic structure • nickel • copper • phosphasalen non-innocent ligands• multi-configurational ground state

[1] C. K. Jorgensen, *Coord. Chem. Rev.* **1966**, *1*, 164-178.

[2] a) V. Lyaskovskyy, B. de Bruin, *ACS Catal.* **2012**, *2*, 270-279; b) W. Kaim, *Inorg. Chem.* **2011**, *50*, 9752-9765.

[3] a) F. Thomas, *Dalton Trans.* **2016**, *45*, 10866-10877; b) S. N. Brown, *Inorg. Chem.* **2012**, *51*, 1251-1260; c) A. L. Smith, K. I. Hardcastle, J. D. Soper, *J. Am. Chem. Soc.* **2010**, *132*, 14358-14360; d) K. Heinze, S. Reinhardt, *Chem. Eur. J.* **2008**, *14*, 9482-9486; e) M. W. Bouwkamp, A. C. Bowman, E. Lobkovsky, P. J. Chirik, *J. Am. Chem. Soc.* **2006**, *128*, 13340-13341; f) S. C. Bart, K. Chlopek, E. Bill, M. W. Bouwkamp, E. Lobkovsky, F. Neese, K. Wieghardt, P. J. Chirik, *J. Am. Chem. Soc.* **2006**, *128*, 13901-13912; g) S. Patra, B. Sarkar, S. M. Mobin, W. Kaim, G. K. Lahiri, *Inorg. Chem.* **2003**, *42*, 6469-6473; h) D. J. Tempel, L. K. Johnson, R. L. Huff, P. S. White, M. Brookhart, *J. Am. Chem. Soc.* **2000**, *122*, 6686-6700.

[4] P. J. Chirik, K. Wieghardt, *Science* **2010**, *327*, 794-795.

[5] a) A. M. Tondreau, C. C. H. Atienza, K. J. Weller, S. A. Nye, K. M. Lewis, J. G. P. Delis, P. J. Chirik, *Science* **2012**, *335*, 567-570; b) S. Monfette, Z. R. Turner, S. P. Semproni, P. J. Chirik, *J. Am. Chem. Soc.* **2012**, *134*, 4561-4564; c) J. M. Darmon, S. C. E. Stieber, K. T. Sylvester, I. Fernandez, E. Lobkovsky, S. P. Semproni, E. Bill, K. Wieghardt, S. DeBeer, P. J. Chirik, *J. Am. Chem. Soc.* **2012**, *134*, 17125-17137.

[6] Y. D. Wang, J. L. DuBois, B. Hedman, K. O. Hodgson, T. D. P. Stack, *Science* **1998**, *279*, 537-540.

[7] a) Y. Shimazaki, *Pure Appl. Chem.* **2014**, *86*, 163-172; b) C. T. Lyons, T. D. P. Stack, *Coord. Chem. Rev.* **2013**, *257*, 528-540; c) Y. Shimazaki, N. Arai, T. J. Dunn, T. Yajima, F. Tani, C. F. Ramogida, T. Storr, *Dalton Trans.* **2011**, *40*, 2469-2479.

[8] a) J. Andrez, V. Guidal, R. Scopelliti, J. Pecaut, S. Gambarelli, M. Mazzanti, *J. Am. Chem. Soc.* **2017**, DOI:10.1021/jacs.1027b03604; b) G. Nocton, P. Horeglad, V. Vetere, J. Pecaut, L. Dubois, P. Maldivi, N. M. Edelstein, M. Mazzanti, *J. Am. Chem. Soc.* **2010**, *132*, 495-508; c) C. Camp, V. Mougel, P. Horeglad, J. Pecaut, M. Mazzanti, *J. Am. Chem. Soc.* **2010**, *132*, 17374-17377.

[9] A. Kochem, H. Kanso, B. Baptiste, H. Arora, C. Philouze, O. Jarjayes, H. Vezin, D. Luneau, M. Orio, F. Thomas, *Inorg. Chem.* **2012**, *51*, 10557-10571.

[10] J. W. Whittaker, *Arch. Biochem. Biophys.* **2005**, *433*, 227-239.

[11] a) R. C. Pratt, C. T. Lyons, E. C. Wasinger, T. D. P. Stack, *J. Am. Chem. Soc.* **2012**, *134*, 7367-7377; b) J. W. Whittaker, *Chem. Rev.* **2003**, *103*, 2347-2363.

[12] T. Storr, P. Verma, R. C. Pratt, E. C. Wasinger, Y. Shimazaki, T. D. P. Stack, *J. Am. Chem. Soc.* **2008**, *130*, 15448-15459.

[13] M. Orio, O. Jarjayes, H. Kanso, C. Philouze, F. Neese, F. Thomas, *Angew. Chemie Int. Ed.* **2010**, *49*, 4989-4992.

[14] K. Asami, K. Tsukidate, S. Iwatsuki, F. Tani, S. Karasawa, L. Chiang, T. Storr, F. Thomas, Y. Shimazaki, *Inorg. Chem.* **2012**, *51*, 12450-12461.

[15] a) D. de Bellefeuille, M. Orio, A.-L. Barra, A. Aukauloo, Y. Journaux, C. Philouze, X. Ottenwaelder, F. Thomas, *Inorg. Chem.* **2015**, *54*, 9013-9026; b) K. Asami, A. Takashina, M. Kobayashi, S. Iwatsuki, T. Yajima, A. Kochem, M. van Gastel, F. Tani, T. Kohzuma, F. Thomas, Y. Shimazaki, *Dalton Trans.* **2014**, *43*, 2283-2293.

[16] W. I. Dzik, J. I. van der Vlugt, J. N. H. Reek, B. de Bruin, *Angew. Chemie Int. Ed.* **2011**, *50*, 3356-3358.

[17] a) R. C. Walroth, J. T. Lukens, S. N. MacMillan, K. D. Finkelstein, K. M. Lancaster, *J. Am. Chem. Soc.* **2016**, *138*, 1922-1931; b) C. M. Lemon, M. Huynh, A. G. Maher, B. L. Anderson, E. D. Bloch, D. C. Powers, D. G. Nocera, *Angew. Chemie Int. Ed.* **2016**, *55*, 2176-2180.

[18] a) M. B. Watson, N. P. Rath, L. M. Mirica, *J. Am. Chem. Soc.* **2017**, *139*, 35-38; b) E. Chong, J. W. Kampf, A. Ariafard, A. J. Canty, M. S. Sanford, *J. Am. Chem. Soc.* **2017**, *139*, 6058-6061; c) G. E. Martinez, C. Ocampo, Y. J. Park, A. R. Fout, *J. Am. Chem. Soc.* **2016**, *138*, 4290-4293; d) J. R. Bour, N. M. Camasso, M. S. Sanford, *J. Am. Chem. Soc.* **2015**, *137*, 8034-8037.

[19] a) J. C. Tellis, C. B. Kelly, D. N. Primer, M. Jouffroy, N. R. Patel, G. A. Molander, *Acc. Chem. Res.* **2016**, *49*, 1429-1439; b) J. R. Bour, N. M. Camasso, E. A. Meucci, J. W. Kampf, A. J. Canty, M. S. Sanford, *J. Am. Chem. Soc.* **2016**, *138*, 16105-16111.

[20] a) J. C. Vantourout, H. N. Miras, A. Isidro-Llobet, S. Sproules, A. J. B. Watson, *J. Am. Chem. Soc.* **2017**, *139*, 4769-4779; b) D. Holt, M. J. Gaunt, *Angew. Chemie Int. Ed.* **2015**, *54*, 7857-7861.

[21] a) C. J. Cramer, W. B. Tolman, *Acc. Chem. Res.* **2007**, *40*, 601-608; b) J. L. DuBois, P. Mukherjee, T. D. P. Stack, B. Hedman, E. I. Solomon, K. O. Hodgson, *J. Am. Chem. Soc.* **2000**, *122*, 5775-5787.

[22] A. D. Spaeth, N. L. Gagnon, D. Dhar, G. M. Yee, W. B. Tolman, *J. Am. Chem. Soc.* **2017**, *139*, 4477-4485.

[23] a) S. N. MacMillan, K. M. Lancaster, *ACS Catal.* **2017**, *7*, 1776-1791; b) N. C. Tomson, K. D. Williams, X. L. Dai, S. Sproules, S. DeBeer, T. H. Warren, K. Wieghardt, *Chem. Sci.* **2015**, *6*, 2474-2487.

[24] A. C. Bowman, C. Milsmann, E. Bill, Z. R. Turner, E. Lobkovsky, S. DeBeer, K. Wieghardt, P. J. Chirik, *J. Am. Chem. Soc.* **2011**, *133*, 17353-17369.

[25] T. L. Gianetti, G. Nocton, S. G. Minasian, N. C. Tomson, A. L. D. Kilcoyne, S. A. Kozimor, D. K. Shuh, T. Tyliszczak, R. G. Bergman, J. Arnold, *J. Am. Chem. Soc.* **2013**, *135*, 3224-3236.

[26] a) Y. Shimazaki, T. Yajima, F. Tani, S. Karasawa, K. Fukui, Y. Naruta, O. Yamauchi, *J. Am. Chem. Soc.* **2007**, *129*, 2559-2568; b) L. Benisvy, R. Kannappan, Y. F. Song, S. Milikisyants, M. Huber, I. Mutikainen, U. Turpeinen, P. Gamez, L. Bernasconi, E. J. Baerends, F. Hartl, J. Reedijk, *Eur. J. Inorg. Chem.* **2007**, 637-642.

[27] a) G. Nocton, W. W. Lukens, C. H. Booth, S. S. Rozenel, S. A. Medling, L. Maron, R. A. Andersen, *J. Am. Chem. Soc.* **2014**, *136*, 8626-8641; b) C. H. Booth, D. Kazhdan, E. L. Werkema, M. D. Walter, W. W. Lukens, E. D. Bauer, Y. J. Hu, L. Maron, O. Eisenstein, M. Head-Gordon, R. A. Andersen, *J. Am. Chem. Soc.* **2010**, *132*, 17537-17549; c) C. H. Booth, M. D. Walter, D. Kazhdan, Y. J. Hu, W. W. Lukens, E. D. Bauer, L. Maron, O. Eisenstein, R. A. Andersen, *J. Am. Chem. Soc.* **2009**, *131*, 6480-6491.

[28] G. Nocton, C. H. Booth, L. Maron, R. A. Andersen, *Organometallics* **2013**, *32*, 5305-5312.

[29] a) N. C. Tomson, M. R. Crimmin, T. Petrenko, L. E. Rosebrugh, S. Sproules, W. C. Boyd, R. G. Bergman, S. DeBeer, F. D. Toste, K. Wieghardt, *J. Am. Chem. Soc.* **2011**, *133*, 18785-18801; b) C. E. Ruggiero, S. M. Carrier, W. E. Antholine, J. W. Whittaker, C. J. Cramer, W. B. Tolman, *J. Am. Chem. Soc.* **1993**, *115*, 11285-11298; c) S. M. Carrier, C. E. Ruggiero, W. B. Tolman, G. B. Jameson, *J. Am. Chem. Soc.* **1992**, *114*, 4407-4408.

[30] a) J. Zapata-Rivera, R. Caballol, C. J. Calzado, *Phys. Chem. Chem. Phys.* **2011**, *13*, 20241-20247; b) J. Zapata-Rivera, R. Caballol, C. J. Calzado, *J. Comput. Chem.* **2011**, *32*, 1144-1158.

[31] a) M. Goswami, V. Lyaskovskyy, S. R. Domingos, W. J. Buma, S. Woutersen, O. Troeppner, I. Ivanovic-Burmazovic, H. J. Lu, X. Cui, X. P. Zhang, E. J. Reijerse, S. DeBeer, M. M. van Schooneveld, F. F. Pfaff, K. Ray, B. de Bruin, *J. Am. Chem. Soc.* **2015**, *137*, 5468-5479; b) A. J. Rosenthal, M. Vogt, B. de Bruin, H. Grutzmacher, *Eur. J. Inorg. Chem.* **2013**, *2013*, 5831-5835.

[32] a) T. Cheisson, A. Auffrant, *Dalton Trans.* **2014**, *43*, 13399-13409; b) T. P. A. Cao, A. Buchard, X. F. Le Goff, A. Auffrant, C. K. Williams, *Inorg. Chem.* **2012**, *51*, 2157-2169; c) A. Buchard, H. Heuclin, A. Auffrant, X. F. Le Goff, P. Le Floch, *Dalton Trans.* **2009**, 1659-1667; d) A. Buchard, A. Auffrant, C. Klemps, L. Vu-Do, L. Boubekeur, X. F. Le Goff, P. Le Floch, *Chem. Commun.* **2007**, 1502-1504.

[33] T. P. A. Cao, S. Labouille, A. Auffrant, Y. Jean, X. F. Le Goff, P. Le Floch, *Dalton Trans.* **2011**, *40*, 10029-10037.

[34] T. P. A. Cao, G. Nocton, L. Ricard, X. F. Le Goff, A. Auffrant, *Angew. Chem. Int. Ed. Engl.* **2014**, *53*, 1368-1372.

[35] a) L. Chiang, A. Kochem, O. Jarjayes, T. J. Dunn, H. Vézin, M. Sakaguchi, T. Ogura, M. Orio, Y. Shimazaki, F. Thomas, T. Storr, *Chem. Eur. J.* **2012**, *18*, 14117-14127; b) T. Storr, E. C. Wasinger, R. C. Pratt, T. D. P. Stack, *Angew. Chemie Int. Ed.* **2007**, *46*, 5198-5201.

[36] a) K. Ray, T. Petrenko, K. Wieghardt, F. Neese, *Dalton Trans.* **2007**, 1552-1566; b) E. Kogut, H. L. Wiencko, L. B. Zhang, D. E. Cordeau, T. H. Warren, *J. Am. Chem. Soc.* **2005**, *127*, 11248-11249.

[37] C. Bakewell, T. P. A. Cao, N. Long, X. F. Le Goff, A. Auffrant, C. K. Williams, *J. Am. Chem. Soc.* **2012**, *134*, 20577-20580.

[38] L. Yang, D. R. Powell, R. P. Houser, *Dalton Trans.* **2007**, 955-964.

[39] J. H. Van Vleck, The Theory of Electric and Magnetic Susceptibilities. Oxford University Press, Oxford, **1932**.

[40] M. Xémard, A. Jaoul, M. Cordier, F. Molton, O. Cador, B. L. Guennic, C. Duboc, O. Maury, C. Clavaguéra, G. Nocton, *Angew. Chem. Int. Ed. Engl.* **2017**, *56*, 4266-4271.

[41] M. D. Walter, M. Schultz, R. A. Andersen, *New J. Chem.* **2006**, *30*, 238-246.

[42] P. Chaudhuri, M. Hess, U. Florke, K. Wieghardt, *Angew. Chemie Int. Ed.* **1998**, *37*, 2217-2220.

[43] F. Thomas, O. Jarjayes, C. Duboc, C. Philouze, E. Saint-Aman, J. L. Pierre, *Dalton Trans.* **2004**, 2662-2669.

[44] H. H. Jaffe, *Chem. Rev.* **1953**, *53*, 191-261.

[45] O. Rotthaus, F. Thomas, O. Jarjayes, C. Philouze, E. Saint-Aman, J. L. Pierre, *Chem. Eur. J.* **2006**, *12*, 6953-6962.

[46] L. Pauling, The Nature of the Chemical Bond, . Cornell University Press, Ithaca, New York, **1960**.

[47] Y. Shimazaki, T. D. P. Stack, T. Storr, *Inorg. Chem.* **2009**, *48*, 8383-8392.

[48] T. Kurahashi, H. Fujii, *J. Am. Chem. Soc.* **2011**, *133*, 8307-8316.

[49] A. Kochem, J. K. Molloy, G. Gellon, N. Leconte, C. Philouze, F. Berthiol, O. Jarjayas, F. Thomas, *Chem. Eur. J.* **2017**, *23*, doi:10.1002/chem.201702010.

[50] G. N. La Mar, J. Horrocks, W. DeW., R. H. Holm, NMR of paramagnetic molecules; principles and applications. (Eds.: G. N. La Mar, J. Horrocks, W. DeW., R. H. Holm), Academic Press, New York, **1973**.

[51] B. Le Guennic, T. Floyd, B. R. Galan, J. Autschbach, J. B. Keister, *Inorg. Chem.* **2009**, *48*, 5504-5511.

[52] E. Lamour, S. Routier, J. L. Bernier, J. P. Catteau, C. Bailly, H. Vezin, *J. Am. Chem. Soc.* **1999**, *121*, 1862-1869.

[53] a) P. J. Alonso, A. B. Arauzo, M. A. Garcia-Monforte, A. Martin, B. Menjon, C. Rillo, M. Tomas, *Chem. Eur. J.* **2009**, *15*, 11020-11030; b) B. R. McGarvey, *Can. J. Chem. Rev. Can. Chim.* **1975**, 2498-2511.

[54] P. Bertrand, La spectroscopie de résonance paramagnétique électronique : fondements. (Ed.: G. sciences), EDP sciences, Les Ulis, **2014**.

[55] a) S. Amabilino, R. J. Deeth, *Inorg. Chem.* **2017**, *56*, 2602-2613; b) M. Swart, *Chem. Phys. Lett.* **2013**, *580*, 166-171.

[56] a) S. Grimme, J. Antony, S. Ehrlich, H. Krieg, *J. Chem. Phys.* **2010**, *132*; b) S. Grimme, *J. Comput. Chem.* **2006**, *27*, 1787-1799; c) V. N. Staroverov, G. E. Scuseria, J. M. Tao, J. P. Perdew, *J. Chem. Phys.* **2003**, *119*, 12129-12137.

[57] J. Muller, T. Weyhermuller, E. Bill, P. Hildebrandt, L. Ould-Moussa, T. Glaser, K. Wieghardt, *Angew. Chemie Int. Ed.* **1998**, *37*, 616-619.

[58] a) J. Kanamori, *J. Phys. Chem. Solids* **1959**, *10*, 87-98; b) J. B. Goodenough, *J. Phys. Chem. Solids* **1958**, *6*, 287-297; c) J. B. Goodenough, *Phys. Rev.* **1955**, *100*, 564-573.

[59] R. B. King, Organometallic Syntheses*, Vol. 1*. Academic Press, New York, **1965**.

[60] A. Altomare, M. C. Burla, M. Camalli, G. L. Cascarano, C. Giacovazzo, A. Guagliardi, A. G. G. Moliterni, G. Polidori, R. Spagna, *J. Appl. Crystallogr.* **1999**, *32*, 115-119.

[61] G. M. Sheldrick, SHELXL-97. Universität Göttingen, Göttingen, Germany, **1997**.

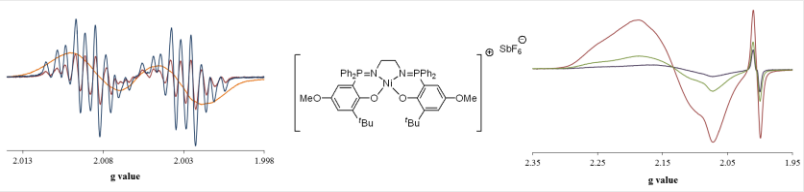

The determination of the electronic structure of one-electron oxidized copper and nickel phosphasalen complexes was carried out combining different experimental techniques and quantum chemistry. A multi-configurational ground state is proposed for these complexes. Indeed, with those non-innocent ligands a small change in the ligand structure modifies the ratio of metal *vs* ligand spin density, which is explained by both electronic and geometrical factors.

I. Mustieles Marín,[a] T. Cheisson,[a] R.Singh Chauhan,[a] C. Herrero,[c] M. Cordier,[a] C. Clavaguéra,[a,b] G. Nocton,[a]* and A. Auffrant[a]**

Page No. – Page No.

Electronic Structures of Mono-Oxidized Copper and Nickel Phosphasalen Complexes